

1 **Stochastic variation in the FOXM1 transcription program mediates replication stress tolerance**

2

3 Hendrika A. Segeren^{1,#}, Kathryn A. Wierenga^{1,#}, Frank M. Riemers^{1,2}, Elsbeth A. van Liere¹, Bart
4 Westendorp^{1*}

5

6 ¹Department of Biomolecular Health Sciences, Faculty of Veterinary Medicine, Utrecht University,
7 Utrecht, The Netherlands.

8 ²Department of Clinical Sciences, Faculty of Veterinary Medicine, Utrecht University, Utrecht, The
9 Netherlands.

10 # equal contribution

11 * Corresponding author; lead contact

12 E-mail address corresponding author: b.westendorp@uu.nl

13

14

15

16 **Abstract**

17

18 Oncogene-induced replication stress (RS) is a vulnerability of cancer cells that forces reliance on the
19 intra-S-phase checkpoint to ensure faithful genome duplication. Inhibitors of the crucial intra-S-phase
20 checkpoint kinases ATR and CHK1 have been developed, but persistent proliferation and resistance to
21 these drugs remain problematic. Understanding drug tolerance mechanisms is impeded by analysis of
22 bulk samples, which neglect tumor heterogeneity and often fail to accurately interpret cell cycle-
23 mediated resistance. Here, by combining intracellular immunostaining and RNA-sequencing of single
24 cells, we characterized the transcriptomes of oncogenic RAS-expressing cells that exhibit variable levels
25 of RS when challenged with a CHK1 inhibitor in combination with the chemotherapeutic drug
26 gemcitabine. We identified 40 genes differentially expressed between tolerant and sensitive cells,
27 including several *FOXM1* target genes. While complete knockdown of *FOXM1* impeded cell proliferation,
28 a partial knockdown protected cells against DNA damage, and improved recovery from drug-induced RS.
29 Our results suggest that low levels of *FOXM1* expression protects subsets of oncogenic RAS-expressing
30 cells against DNA damage during drug-induced replication stress.

31

32

33

34 Introduction

35 Oncogene-induced replication stress (RS) is a vulnerability of cancer cells that can be exploited by anti-
36 cancer therapies. Seminal studies in the beginning of this century already showed that oncogenes, such
37 as RAS, induce DNA damage in precancerous lesions (Bartkova et al., 2006, Gorgoulis et al., 2005).
38 Further research revealed that oncogene-induced RS underlies the elevated levels of DNA damage, and
39 that RS is present in the vast majority of human tumors. As a result, RS is proposed as an emerging
40 hallmark of cancer (Macheret, Halazonetis, 2015b).

41 RS is defined as stalling of the replication fork, which can arise due to shortage of substrates, collisions
42 between replication and transcription machinery, or DNA lesions or secondary structures that hinder the
43 replication machinery. Unresolved RS can progress to replication fork collapse, resulting in single- and
44 double-stranded DNA breaks. To prevent this, cells respond to RS by triggering the intra S-phase
45 checkpoint. Briefly, this checkpoint is initiated when Replication Protein A (RPA) binds to single-stranded
46 DNA that is exposed upon uncoupling of helicase and polymerase activity during fork stalling. This
47 triggers recruitment and activation of ATR and its downstream kinase CHK1, which together induce a
48 cascade of kinase activation that acts to stabilize and repair the stalled replication fork, fire dormant
49 origins in the vicinity of the stalled fork, attenuate global DNA replication and slow down cell cycle
50 progression. This multifaced response ensures faithful genome duplication before mitosis (Lecona,
51 Fernandez-Capetillo, 2018).

52 In general, loss of ATR or CHK1 is lethal in cells where oncogenes are activated (Murga et al., 2011, Gilad
53 et al., 2010, Oo et al., 2018, Schoppy et al., 2012). On the basis of this knowledge, inhibitors against key-
54 players of the intra S-phase checkpoint are developed and currently evaluated in clinical trials (Baillie,
55 Stirling, 2021). To potentiate the effect of intra S-phase checkpoint ablation, ATR and CHK1 inhibitors can
56 be combined with a low dose of chemotherapeutic drugs (Liu et al., 2017, Wallez et al., 2018). However,
57 drug resistance remains a major problem (Hong et al., 2018). The limited *in vivo* activity of drugs which
58 exacerbate RS suggests that cancer cells employ strategies to tolerate RS. Indeed, stabilization of the
59 replication fork (Bianco et al., 2019), increased expression of RPA (Bélanger et al., 2018), and increased
60 dormant origin firing (Jo et al., 2021) grant RS tolerance. Interestingly, factors that curb RS in cancer cells,
61 such as CLASPIN, CHK1, and NRF2, frequently display increased transcript levels in cancer cells (Bianco et
62 al., 2019, Bertoli et al., 2016, Mukhopadhyay et al., 2020). Moreover, unbiased screening approaches
63 uncovered that cell cycle related genes mediate resistance to intra S-phase checkpoint inhibitors

64 (Blosser et al., 2020, Schleicher et al., 2020, Ruiz et al., 2016). However, since these studies employed
65 bulk sample approaches, transcriptional heterogeneity was neglected, rare resistance-conferring events
66 missed, and the role of cell cycle progression potentially misinterpreted. As a result, the development of
67 novel clinical strategies based on these studies is rare.

68 The importance of single-cell data in drug-resistance studies is highlighted by Shaffer *et al.*, who unveil
69 that rare cancer cells express resistance genes prior to treatment to resist therapy (Shaffer et al., 2017).
70 In support of this notion, treatment with RS-inducing drugs leads to a reduction in the number of
71 transcriptionally distinct clones (Seth et al., 2019), suggesting selection pressure for cells harboring drug-
72 tolerant characteristics. Besides pre-existing heterogeneity, it is becoming increasingly evident that
73 cancer cells modulate their transcriptome upon treatment to circumvent therapy. For example,
74 chemotherapeutic drugs may induce a transient drug-tolerant state in a subpopulation of cells (Goldman
75 et al., 2015, Rehman et al., 2021). It is hypothesized that this provides a time window in which
76 permanent resistant cells can arise. Because transcriptional heterogeneity could result in resistance to
77 RS-inducing drugs and consequently tumor relapse, the mechanisms underlying RS tolerance warrant
78 further investigation.

79 Here, we employed a strategy in which we combine immunostaining of RS markers and information on
80 cell cycle phase with single cell RNA-sequencing. This allowed us to shed light on the biological variability
81 in response to RS. We uncovered a subset of genes with an altered expression profile in cells that
82 maintained low levels of RS despite challenge with RS-inducing drugs. We also identified genes that
83 make cells more sensitive to replication stress, which included several FOXM1 target genes. Consistent
84 with this, partial knockdown of FOXM1 mitigated DNA damage and improved cell survival following
85 treatment with RS-inducing drugs. These findings provide potential new avenues for development of
86 synthetic lethality strategies and identification of biomarkers to optimize anti-cancer therapy.

87

88 Results

89 *γH2AX is a replication stress marker suitable for flow cytometry of DSP-fixed cells*

90 To unmask transcription mediated RS-adaptation mechanisms, transcriptomic information and the level
91 of RS in single cells needs to be combined. Therefore, we adapted a previously published strategy in
92 which cells are reversibly fixed to allow antibody staining while preserving RNA for sequencing (Gerlach
93 et al., 2019). As summarized in Fig. 1A, cells were fixed using the chemically reversible crosslinking
94 reagent DSP. Next, cells were stained with an antibody that recognizes an RS-specific marker and sorted
95 based on RS levels in 384-well plates using FACS. Subsequently, de-crosslinking was performed using the
96 reducing agent DTT and cells were subjected to first strand cDNA synthesis and single-cell RNA-
97 sequencing.

98 Before implementation of this technique, we first investigated which antibody against RS-induced
99 protein modifications is compatible with DSP-fixation and analysis by flow-cytometry. To induce RS, we
100 employed the frequently used chemotherapeutic drug gemcitabine in combination with the CHK1
101 inhibitor (CHK1i) prexasertib (Segeren et al., 2022). In response to RS, the intra S-phase checkpoint
102 kinase ATR is activated to stabilize and repair stalled forks and delay cell cycle progression. This is
103 mediated by a sequence of events including phosphorylation of CHK1, RPA2, KAP1 and H2AX (Toledo et
104 al., 2013, Branigan et al., 2021). Antibodies against phosphorylated variants of these proteins are
105 previously shown to detect increased levels of RS by flow-cytometry (Atashpaz et al., 2020, Branigan et
106 al., 2021). We assessed if these antibodies could detect an increase in phosphorylated CHK1, RPA2, KAP1
107 and H2AX in DSP-fixed cells after treatment with CHK1i + gemcitabine.

108 We made use of RPE-1 cells harboring a doxycycline-inducible variant of oncogenic RAS (hereafter
109 referred to as RPE-HRAS^{G12V} for cells with doxycycline-induced expression of HRAS^{G12V} or control for their
110 non-induced counterparts). (Segeren et al., 2022). The advantage of this system is that adaptation to RS
111 can be studied in the frequently occurring oncogenic context of RAS hyperactivation, while the effect of
112 other tumor-specific mutations is excluded. We previously described that RPE-HRAS^{G12V} cells show mild
113 endogenous RS and markedly enhanced sensitivity to CHK1i + gemcitabine (Segeren et al., 2022)).
114 However, control RPE cells also show RS in presence of high doses of these drugs. Accordingly, treating
115 RPE control cells with a high dose of CHK1i + gemcitabine resulted in 2N-cell cycle arrest, as seen by the
116 accumulation of cells with low DAPI signal, indicating severe stress. CHK1i + gemcitabine also triggered
117 an abundant increase in phosphorylated KAP1, RPA2 and H2AX (Fig. 1B). However, the tested antibody

118 against phospho-Serine 345 on CHK1 failed to show an increase in this flow cytometric analysis of DSP
119 fixed cells, excluding it as an RS-marker for this project (Fig. 1B). While KAP1 mediates RS-induced DNA
120 remodeling and RPA2 protects stalled replication forks, phosphorylated H2AX is present at collapsed
121 replication forks (Goodarzi, Jeggo & Kurka, 2011, Toledo et al., 2013). Since the latter is the most
122 downstream event in the RS-cascade and indicates severe RS, the antibody against phosphorylated H2AX
123 Serine 139 (hereafter referred to as γ H2AX) was selected as a proxy for RS-induced DNA damage.
124 Interestingly, flow-cytometry analysis of γ H2AX stained cells revealed great diversity in the signal, and
125 presumable RS-level, between individual cells (Fig. 1B, inset). Consistent with this, heterogenous
126 phosphorylation of H2AX S139 in response to RS was confirmed by immunofluorescence staining (Fig.
127 1C). In addition, immunoblotting confirmed that substantial γ H2AX was observed when the CHK1i
128 prexasertib was combined with a low dose of gemcitabine, but not with either drug alone (Fig. 1D).
129 Based on these observations, we concluded that the antibody against γ H2AX can be used to determine
130 the level of RS induced by CHK1i and gemcitabine at a single cell resolution in DSP-fixed cells.

131

132 *High quality single-cell RNA sequencing data of fixed cells with known level of replication stress*

133 After identification of γ H2AX as an RS-marker we directly compared fresh and DSP fixed cells to evaluate
134 the extent to which fixation with DSP affects the quality of single-cell RNA sequencing data. Since the
135 response to RS is affected by cell cycle stage, we decided to sort only cycling cells. To this end we made
136 use of the fact that our RPE-HRAS^{G12V} cells stably expressed the Fluorescent Ubiquitination-based Cell
137 Cycle Indicator (FUCCI4) system (Bajar et al., 2016). We sorted RPE-HRAS^{G12V} cells expressing Geminin<sub>1-
138 110</sub>, representing S/G2-phase, with and without treatment with RS-inducing drugs. Half of the cells were
139 directly sorted (fresh), whereas the other half was first fixed with DSP and stained using the
140 aforementioned γ H2AX antibody. All samples were subjected to standard cDNA preparation, including
141 de-crosslinking, and RNA-sequencing. After initial quality control (described in methods section), 232
142 fresh (success rate = 60.42%) and 273 DSP-fixed (success rate = 71.09%) cells were selected for
143 downstream analysis. The mean number of identified genes (5644 in fresh versus 5044 in DSP-fixed cells)
144 was comparable (Fig. 2A), as was RNA count, percentage of mitochondrial genes, and spike-in RNAs (Fig.
145 S1A-C). Moreover, the average gene expression and gene detection rate were not affected by DSP-
146 fixation (Fig. 2B-C). In addition, the similar coefficients of variation in the two cell populations indicates
147 that DSP-fixation does not negatively impact the ability to detect expression heterogeneity (Fig. 2D).

148 After confirming that we can obtain high quality single cell RNA sequencing data from DSP-fixed cells, we
149 aimed to identify gene-expression programs that mediate the low level of RS in a subset of cells and
150 potentially underly drug resistance. However, when we analyzed cells treated with Chk1i + gemcitabine,
151 the γ H2AX positive and negative cells do not clearly cluster apart in the tSNE plot shown in Fig. 2E. Thus,
152 not the level of RS, but other factors account for the clustering within the DSP-fixed cell population. To
153 assess if cell cycle status can explain the clustering, we plotted the protein level of the FUCCI4 cell cycle
154 marker Geminin₁₋₁₁₀. The protein level of Geminin₁₋₁₁₀, which gradually increases during S-phase
155 progression, correlated well with the different cell clusters, suggesting that transcriptional events
156 underlying S and G2 phase account for clustering (Fig. 2F). Accordingly, the expression of early S-phase
157 (*CDC6* and *E2F1*) and late G2/M-phase (*PLK1* and *CCNB1*) markers showed that high levels of RS are
158 predominantly present in cells in late S or G2 phase (Fig. 2G). Thus, cell cycle position can be a major
159 confounding factor when evaluating the transcriptomic response to RS.

160

161 *Identification of putative genes that confer replication stress tolerance*

162 To reduce the variation in level of RS caused by cell cycle status, we more stringently selected cells solely
163 in mid S-phase based on the DNA content using DAPI (Fig. 3A). Subsequently, we selected S-phase cells
164 negative for γ H2AX, and S-phase cells with low, medium or high levels of γ H2AX using flow cytometry
165 before and 16h after treatment with RS-inducing drugs. As seen previously (Fig. 1C), treatment with
166 CHK1i + gemcitabine increased the level of γ H2AX in RPE-HRAS^{G12V} cells, but several cells still maintained
167 low levels of γ H2AX (Fig. 3A). Hence, to allow identification of mechanisms that facilitate resistance to
168 RS-inducing drugs, we collected cells with no, low, intermediate or high levels of γ H2AX staining for
169 single-cell RNA-sequencing.

170 In an attempt to identify the influence of oncogenic RAS on transcriptional mechanisms of resistance, we
171 similarly treated RPE-HRAS^{G12V} and control RPE cells with CHK1i + gemcitabine and sorted cells with
172 different levels of RS. We subjected these cells to single-cell RNA sequencing and selected cells with
173 more than 1000 unique RNA counts and expressing at least 500 genes for downstream analysis (exact
174 parameters stated in Methods section). Next, we performed principal component analysis and t-SNE
175 visualization. This revealed eight distinct clusters of cells that correlated well with the different
176 experimental conditions (Fig. 3B,C). Interestingly, rare cells treated with CHK1i + gemcitabine are located
177 within the untreated cell cluster (Fig. 3C), potentially representing non-damaged, RS-tolerant cells.

178 Moreover, CHK1i + gemcitabine treated cells in cluster 0 and 4 display lower levels of RS compared to
179 cells in cluster 2 and 3 (Fig. 3A-D).

180 To rule out the influence of cell cycle position, we compared the DAPI signal, indicative of S-phase
181 progression, in cells with different levels of γ H2AX signal. The DAPI signal was comparable in cells with
182 low, medium, and high levels of RS, but the DAPI signal was much lower in γ H2AX^{negative} cells (Fig. S2A).
183 Because we suspected that the absence of RS in γ H2AX^{negative} cells could be attributed to their earlier
184 position in S-phase, we chose to compare the transcriptomes of γ H2AX^{low} and γ H2AX^{high} RPE-HRAS^{G12V}
185 cells. We suspect that cells able to withstand DNA damage during replication stress represent cells within
186 in a tumor that could survive treatment with RS-inducing drugs. Differential expression analysis revealed
187 19 genes that were significantly downregulated in γ H2AX^{low} RPE-HRAS^{G12V} cells, suggesting that elevated
188 levels of these genes are correlated with sensitivity to RS-inducing drugs (Fig. 3E and Table S1). A large
189 subset of these genes (*CENPE*, *UBE2C*, *HMGB2*, *ANLN* and *MKI67*) are controlled by the key G2/M
190 transcription factor FOXM1 (Fischer, Martin et al., 2016). In contrast to genes with a reduced expression
191 in γ H2AX^{low} cells, 18 genes, including several P53 target genes, had significantly higher expression in
192 γ H2AX^{low} cells, and thus correlated with RS tolerance (Fig. 3F and Table S1).

193 Next, we evaluated if the genes differentially expressed in γ H2AX^{high} versus γ H2AX^{low} cells are co-
194 expressed (Fig. S2B). Among genes downregulated in γ H2AX^{low} cells, the expression of *ANLN*, *HMGB2*,
195 *CENPE*, *MKI67* and *UBE2C* correlated, which is expected as they are all regulated by the FOXM1
196 transcription factor. However, no co-expression of the putative RS-tolerance conferring genes, genes
197 upregulated in γ H2AX^{low} cells, was observed. This indicates that these genes are regulated independently
198 of each other.

199 Notably, several FOXM1-target genes were also found to be downregulated in the γ H2AX^{low} RPE control
200 cells that lack expression of oncogenic RAS (Fig. S2C). This suggests that reduced activation of this
201 transcriptional program in cells with decreased γ H2AX levels is a general phenomenon and not
202 necessarily linked to oncogene expression.

203 Altogether, these data indicate that a subset of oncogenic RAS expressing cells is protected from RS upon
204 treatment with RS-inducing drugs and that these cells transcriptionally diverge from drug-sensitive cells,
205 with many differentially expressed genes targeted by the transcription factor FOXM1.

206

207 *Validation of putative RS tolerance mechanisms*

208 Next, we assessed if the aforementioned genes that were differentially expressed in γ H2AX^{low} versus
209 γ H2AX^{high} RPE-HRAS^{G12V} cells could be functionally responsible for RS sensitivity and RS tolerance (Fig.
210 4A). To this end we knocked down these genes individually prior to treatment with CHK1i + gemcitabine
211 and analyzed if this affected RS. We hypothesized that knocking down sensitizing genes would result in a
212 decrease in replication stress while knocking down tolerizing genes would result in an increase in RS
213 upon treatment with CHK1i+gemcitabine (Fig. 4A). We excluded P53 target genes (*MDM2*, *SERPINE1*,
214 *SNX5*, *FOSL1*, *MT-CO3*) as the key role of P53 in the RS response is well-established (Macheret,
215 Halazonetis, 2015a). Moreover, individual FOXM1 target genes (*CENPE*, *UBE2C*, *HMGB2*, *ANLN*, *MKI67*)
216 were excluded from further analysis and replaced by knockdown of *FOXM1* itself to address the role of
217 this entire transcription program in the RS-response (Fischer, M., 2017, Fischer, Martin et al., 2016).

218 First, we confirmed that small interfering RNAs (siRNAs) targeting the putative RS-sensitizing
219 mechanisms efficiently depleted their target gene (Fig. S3A). For initial siRNA knockdowns, we used
220 siRNA Smartpools, which consist of four unique siRNAs targeting the same gene. Since RS-inducing drugs
221 only affect replicating cells, we sought to enrich the cell population for cells in late S/G2 phase of the cell
222 cycle at the time of analysis. To this end, we depleted the gene of interest using siRNA and arrested all
223 cells in G1-phase using the CDK4/6 inhibitor palbociclib. Subsequently, we released the cells from
224 palbociclib in the presence of CHK1i + gemcitabine and evaluated the level of RS 14 hours after release,
225 when most cells were in late S/G2 phase (Fig. S3B). In addition to enriching for late S/G2 phase cells, this
226 approach ensured that all cells start DNA replication in the presence of CHK1i + gemcitabine. To exclude
227 bias from cells that failed to enter S-phase after palbociclib release when evaluating the level of RS, we
228 calculated the γ H2AX positive cells as percentage of the Geminin₁₋₁₁₀ positive (i.e., S/G2-phase) cells.

229 We first evaluated if depletion of genes upregulated in γ H2AX^{low} cells could resensitize cells to RS (Fig.
230 4A). While depletion of most putative RS-tolerance genes using Smartpool siRNAs did not affect RS,
231 depletion of *MYL6*, *PRDX5* and *ARL4C* increased RS induced by CHK1i + gemcitabine (Fig. S3C). However,
232 when we then used individual siRNAs to deconvolute the effects of the Smartpools, none of the three
233 targets showed a consistent RS-sensitizing effect, suggesting off-target effects of the individual siRNAs
234 (data not shown).

235 We then shifted our focus to genes that may make cells more sensitive to RS. *AMOTL2*, *CTGF* and *CYR61*
236 were downregulated in γ H2AX^{low} cells and knockdown reduced the fraction of cells with severe RS (Fig.

237 S3C). This suggests that these genes sensitize cells to RS-inducing drugs. Similarly, knockdown of *FOXM1*,
238 which regulates the expression of a panel of sensitizing genes (*CENPE*, *UBE2C*, *HMGB2*, *ANLN*, *MKI67*)
239 bolstered resistance to RS induced by CHK1i + gemcitabine (Fig. SC3). However, only *FOXM1* knockdown
240 passed the deconvolution step, i.e., consistent phenotypes with individual siRNAs.

241 We observed varying levels of *FOXM1* knockdown with the four siRNAs against *FOXM1* present in the
242 siRNA Smartpool, with two siRNAs accomplishing a near-complete knockdown (<90%) and two
243 accomplishing a modest knockdown (50-60%) of the gene (Fig. 4B). The siRNAs that produced stronger
244 *FOXM1* knockdown also slowed cell cycle progression, as seen by a lower proportion of cells in G2 phase
245 at 14 hours following release from G1 arrest (Fig. 4C, top row). Despite the differential degrees of
246 *FOXM1* expression and cell cycle progression, all four knockdowns resulted in decreased levels of γ H2AX
247 relative to cells transfected with scrambled siRNA after 14 hr of CHK1i + gemcitabine treatment in
248 synchronized RPE-HRAS^{G12V} cells (Fig. 4C, bottom row; quantified in Fig. S4).

249 We then performed clonogenic survival assays in cells with varying *FOXM1* gene expression levels during
250 treatment with CHK1i + gemcitabine (Fig. 4D,E). The transient effect of siRNA knockdown allowed us to
251 focus on the consequence of reduced FOXM1 expression at the time of treatment (mimicking stochastic
252 variation in expression levels that may occur in cancer cells) rather than a permanent change in
253 expression levels. We quantified colony outgrowth using the IntensityPercent value calculate by the
254 ImageJ ColonyArea plugin, which takes into account both the area covered by cells as well as the density
255 of the cells within a colony (Guzman et al., 2014). In untreated cells, the greater knockdown (siRNA#3
256 and siRNA#4) resulted in fewer colonies, which is expected since knockdown of *FOXM1* slows cell
257 proliferation. The partial knockdown had little to no effect on colonies in untreated cells, consistent with
258 the minimal effect on cell cycle progression. In the scrambled condition, treatment with CHK1i +
259 gemcitabine nearly suppressed the outgrowth of colonies once the drugs were removed. However, in the
260 partial knockdowns, several dense colonies were able to recover even following drug exposure,
261 suggesting that the partial knockdown of FOXM1 protected cells from RS-induced cell death without
262 limiting cell proliferation.

263 To summarize, these data indicate that partial FOXM1 knockdown protects against drug-induced RS
264 while still allowing cells to proliferate. This suggests that cancer cells may use similar tuning of the
265 FOXM1 expression program to resist the effects of RS-inducing drugs without fully halting growth.

266

267

268

269 Discussion

270 In this study, we used single cell RNA sequencing to investigate transcriptional heterogeneity associated
271 with differential responses to RS. We employed a novel technique wherein cells are reversibly fixed,
272 allowing for cell sorting based on intracellular staining, and subsequent single cell RNA sequencing on
273 sorted cells. By comparing cells with low levels of RS (as measured by γ H2AX following treatment with
274 RS-inducing drugs) to cells with high levels of RS, we found that a moderate reduction in gene expression
275 of downstream targets of transcription factor *FOXM1* protects cells against RS induced by
276 CHK1i+gemcitabine without significantly delaying cell proliferation.

277 Compared to popular screening approaches such as CRISPR or RNA interference libraries, our approach
278 has caveats. First, a differentially expressed gene in RS-tolerant versus RS-sensitive cells can be either a
279 cause or a consequence of the observed phenotype. Our observation that P53 target genes were
280 downregulated in RS-tolerant cells illustrates this issue (Figure 3E, S2C). The far majority of our potential
281 hits did not show consistent phenotypes when knocked down with siRNA, suggesting that they do not
282 play a direct role in regulating RS. Second, genes may act in concert: the effect of the variation in
283 expression of an individual gene can be minimal, while up- or down-regulation of multiple genes can
284 have a tolerizing effect. Further studies altering the levels of multiple genes at once would be necessary
285 to test this hypothesis. Nevertheless, our single cell transcriptomics approach has the advantage over the
286 aforementioned screening approaches that it has the potential to detect the effects of stochastic
287 heterogenous transcription events within the physiological range.

288 We observed that reducing *FOXM1* expression improves cell viability (as seen by colony outgrowth)
289 following treatment with RS-inducing drugs. This is consistent with recent studies showing that high
290 *FOXM1* activity facilitates unscheduled mitotic entry to cause RS-induced mitotic catastrophe (O'Brien et
291 al., 2023, Gallo et al., 2022, Chung et al., 2019, Branigan et al., 2021). *FOXM1* primes cells to enter
292 mitosis by inducing the transcription of a large set of mitotic genes, including *CCNB1*, *PLK1* and *CDK1*
293 itself which allows for sufficient accumulation and activation of cyclin B-CDK1 complexes to enter mitosis
294 (Sanders et al., 2015, Sadasivam, Duan & DeCaprio, 2012). Curtailing CDK1 activation reduces sensitivity
295 to RS response inhibitors because cells are less prone to enter mitosis prematurely with DNA damage
296 sustained during RS. This can be reversed by inhibiting key regulators of CDK1 activity, such as *WEE1*,
297 thus reactivating CDK1 (Ruiz et al., 2016).

298 In addition to highlighting the described role of FOXM1 in promoting mitotic catastrophe, this study also
299 points to a RS-mediating activity of FOXM1 during S-phase. Our finding that low FOXM1 expression
300 reduces CHK1i-mediated DNA damage is consistent with recent observations showing that FOXM1
301 deletion reduced replication stress and DNA damage in S-phase during CHK1i treatment (Branigan et al.,
302 2021). Remarkably, Branigan and co-workers observed no effect of full FOXM1 deletion on cell cycle
303 progression, whereas we observed that near-complete knockdown of FOXM1 caused a clear reduction of
304 S phase progression and proliferation rates (Figure 4B, C; siRNAs #3 and #4). A difference could be that
305 FOXM1-mutant cells have adapted to chronic loss of this transcription factor in the former study, where
306 RNAi-mediated knockdown provides a more acute setting. Notwithstanding these differences, the
307 mechanism by which high FOXM1 activity is a prerequisite to accumulate DNA damage in S-phase during
308 CHK1 inhibition remains to be uncovered. One possible explanation could be that high FOXM1
309 expression triggers excessive origin firing during CHK1 inhibition. An important function of CHK1 is to
310 mitigate DNA damage by reducing firing of late origins under conditions of replication stress (Baillie,
311 Stirling, 2021). Cyclin A2-CDK1 complexes mediate origin firing, and *CCNA2* is a FOXM1 target (Katsuno et
312 al., 2009), thus FOXM1-induced *CCNA2* expression exacerbate the increase in late origin firing permitted
313 by CHK1 inhibition. Consistent with this, a recent study using ATR-deficient B cells showed that RS
314 triggered by loss of ATR could be reversed by suppressing origin firing, which was accomplished through
315 partial inhibition of CDC7 and CDK1 activity (Menolfi et al., 2023).

316 The work described here describes a model in which transcriptomic variability of the transcription factor
317 FOXM1 endows a subset of cells within a population of genetically identical cells tolerance to drug-
318 induced replication stress. While it may be hard to therapeutically target FOXM1 to improve efficacy of
319 intra-S-phase checkpoint inhibitors, overexpression of the FOXM1 program can potentially serve as a
320 biomarker since amplification of the FOXM1 gene occur relatively frequently in multiple cancers (Barger
321 et al., 2019), although single cell analysis would need to reveal the relative heterogeneity within tumors.
322 Furthermore, our findings support the idea that decelerated S-phase progression could counteract CHK1
323 inhibitors, which also suggests that pharmacologically accelerating cell cycle progression may work to
324 sensitize cells to this class of drugs. An excellent example of this is inhibiting WEE1, the kinase
325 responsible for preventing CDK1/2 activation or its relative PKMYT1, which inhibits CDK2. WEE1 and
326 PKMYT1 inhibitors force cell proliferation in the presence of RS and – at least in part – overcome
327 resistance to intra S-phase checkpoint inhibitors (Ruiz et al., 2016, Chung et al., 2019, Koh et al., 2018).

328

329 **Methods**

330 *Key resources*

331 Key resources are listed in Table S1.

332

333 *Cell lines*

334 hTERT RPE-1 cell line was obtained from ATCC and cultured at 37°C, 5% CO₂ in DMEM supplemented
335 with 10% FBS and 1% pen/strep. Cell lines were regularly tested and confirmed mycoplasma negative.

336 Overexpression of HRAS^{G12V} was induced by adding 0.2 µg/mL doxycycline to the culture medium.

337 Gemcitabine, prexasertib and palbociclib were purchased from Selleck chemicals and used at a final
338 concentration of 4 nM, 10 nM and 1 µM respectively, unless stated otherwise.

339 RPE cell lines harboring the Tet Repressor, doxycycline inducible HRAS^{G12V}, FUCCI4 system and
340 fluorescent tagged truncated 53BP1 were created using the third-generation lentiviral packaging system
341 as previously described (Segeren et al., 2022).

342

343 *DSP fixation and antibody staining of single cells*

344 Fixation of cells was performed according to the protocol described by Gerlach *et al.* (Gerlach et al.,
345 2019). In short, cells were collected by trypsinization, washed with PBS after which cells were fixed with
346 0.5mM dithiobis(succinimidyl propionate) (DSP) in Sodium Phosphate buffered Saline (pH 8.4) for 45
347 minutes at room temperature at a concentration of 1 million cells per 2.5mL. Next, DSP was neutralized
348 by incubating the cells with quench buffer (100mM Tris, pH 7.5, 150mM NaCl) for 10 minutes and cell
349 clumps were removed using a 70 µm cell strainer. Cells were incubated for 30 minutes with BP buffer
350 (PFBB:PBS, 1:1, supplemented with 0.1% Triton X-100) to permeabilize the cells, after which samples
351 were incubated overnight with antibodies in BP buffer. If samples were intended to use for single-cell
352 RNA-sequencing, BP buffer was supplemented with 2 U/µl RNAsin Plus. Samples were filtered using a
353 40µm cell strainer and incubated with DAPI (0.2µg/mL) prior to loading of samples on the flow
354 cytometer.

355 For antibody testing, samples were loaded on a CytoFLEX flow cytometer and analyzed using FlowJo
356 v10.0 software. Index sorting of cells for single-cell RNA-sequencing was performed on a BD Influx cell
357 sorter.

358

359 *Microscopy*

360 For immunofluorescence staining, cells were seeded on coverslips. Prior to fixation of cells using 4%
361 paraformaldehyde for 20 minutes, pre-extraction with 0.2% Triton X-100 for 1 minute on ice was
362 performed. Next, cells were permeabilized using 0.1% Triton X-100 for 10 minutes, blocked with 5% goat
363 serum and incubated with indicated antibodies after which coverslips were mounted on slides. Samples
364 were analyzed on a Leica SP8 confocal microscope equipped with a 20x objective. Antibodies and
365 dilutions used are listed in Table S2.

366

367 *Immunoblotting*

368 For immunoblotting, cells were washed twice with ice-cold PBS and lysed in ice-cold RIPA-buffer (50 nM
369 Tris-HCl pH 7.5, 1 mM EDTA, 150 mM NaCl, 0.25% deoxycholate, 1% NP-40) supplemented with NaF (1
370 mM), NaV_3O_4 (1 mM) and protease inhibitor cocktail (11873580001, Sigma Aldrich) after which samples
371 were subjected to a standard SDS-page immunoblot. Antibodies used and dilutions are listed in Table S3.

372

373 *RNAi transfections*

374 For siRNA experiments, cells were transfected with siRNA targeting the gene of interest or a scrambled
375 control using Lipofectamine RNAiMAX according to manufacturers' instructions (Life Technologies,
376 13778030). ON-TARGETplus SMARTpool siRNAs were purchased as custom cherry-pick libraries from
377 Dharmacon and used at a final concentration of 10 nM, while individual siRNAs were used at a final
378 concentration of 1 nM. Efficient knock-down of intended target was confirmed by quantitative PCR 24
379 hours after transfection.

380

381 *Fixation and staining to validate hits with flow cytometry*

382 Cells were collected by trypsinization, washed with PBS, transferred to a 96 well plate and fixed using 4%
383 PFA for 30 minutes while gently shaking. Next, cells were washed with 0.1% BSA in PBS and
384 permeabilized using 0.1% Triton for 30 minutes. Cells were washed once more with 0.1% BSA in PBS
385 prior to incubation with the fluorescent linked γ H2AX antibody for 1 hour at room temperature. DAPI
386 was added to the samples at a final concentration of 2.0 μ g/100,000 cells to stain DNA content. Samples
387 were loaded on a CytoFLEX flow cytometer and analyzed using FlowJo v10.0 software.

388

389 *Clonogenic survival assays*

390 Cells were seeded at low density (200 cells per 12 well plate) to assess colony formation. Following 24
391 hour transfection with 1 nM siRNAs targeting FOXM1, cells were treated with 2 nM prexasertib and 4
392 nM gemcitabine. After 48 hr exposure to the drugs, media was replaced with drug-free media and
393 remaining cells were allowed to grow out to form colonies. The ImageJ ColonyArea plug-in was used to
394 quantify the area of the well covered by colonies as previously described (Guzman et al., 2014).

395

396 *Quantitative PCR*

397 RNA isolation, reverse transcription and quantitative PCR were performed according to manufacturers'
398 instructions using the QIAGEN RNeasy kit, Thermo Fisher cDNA synthesis kit and Bio-RAD SYBR Green
399 Master mix, respectively. Quantification of relative gene transcript levels was performed using the $\Delta\Delta$ Ct
400 method for multiple-reference gene correction using GAPDH or β -Actin and RPS18 as reference genes.
401 Primers used in this manuscript are listed in Table S3.

402

403 *Single-cell RNA-sequencing*

404 For single-cell RNA-sequencing single cells were collected in 384-well plates containing barcoded CEL-
405 seq2 primers and nucleotides using index sorting and stored at -80°C until further processing.

406 De-crosslinking of the DSP fixed cells was performed by addition of 0.1M DTT to the reverse transcription
407 mix (10 mM DTT final concentration), which is part of the regular reverse transcription mix for unfixed
408 cells. SORT-seq sequencing and read alignment were performed by Single Cell Discoveries (Utrecht, the
409 Netherlands) using their pipeline based on CEL-Seq2 (Muraro et al., 2016, Hashimshony et al., 2016).
410 Briefly, samples were barcoded with CEL-seq2 barcodes and UMI during reverse transcription and pooled
411 after second strand synthesis. The resulting cDNA was amplified with an overnight in vitro transcription
412 reaction. From this amplified RNA, sequencing libraries were prepared with Illumina TruSeq small RNA
413 primers, which were paired-end sequencing on the Illumina NextSeq500 platform. Read 1 was used to
414 identify the Illumina library index and CEL-seq2 sample barcode. Read 2 was aligned to the human
415 genome (hg38) transcriptome using the Burrows–Wheeler Aligner v0.7.17 . Reads that mapped equally
416 well to multiple locations were discarded. Mapping and generation of count tables were done using the
417 MapAndGo2 script. Downstream processing and analysis were performed in Rstudio (Version 1.4.1106)
418 and R (Version 4.0.5) using the Seurat package (Version 3.2.3) (Stuart et al., 2019). Cells were filtered and
419 selected for downstream analysis when the following parameters were met: number of detected genes >
420 1000 and < 10,000, Unique Molecular Identifier (UMI) counts > 3,000 and < 75,000, and the percentage
421 of mitochondrial counts and ERCC RNA spike-ins below 25 and 5 respectively. Next, raw counts were
422 normalized, and variance stabilized using the SCTransform method (Hafemeister, Satija, 2019).
423 Subsequently, dimension reduction was performed by principal component analysis. Identified clusters
424 were visualized with t-Distributed Stochastic Neighbor Embedding (t-SNE). Differentially expressed genes
425 were identified using the Seurat FindAllMarkers() function with one non default argument, min.pct =
426 0.25 requiring a greater fraction of cells within a cluster to have expression. After this the results were
427 filtered at a Bonferroni adjusted significance level of $p < 0.05$. Expression correlation between the
428 differentially expressed genes was determined using Pearson correlation. All sequencing data generated
429 in this study are available on the Gene Expression Omnibus under accession numbers GSE256134 and
430 GSE250285.

431

432 *Quantification and statistical analysis*

433 Flow cytometry, immunoblot and quantitative PCR experiments were performed three times unless
434 indicated otherwise. Details on sample size and statistical methods employed are described in the figure
435 legends. * $p < 0.05$, ** $p < 0.01$, *** $p < 0.001$ unless indicated otherwise.

436

437

438 **Acknowledgements**

439 We thank Reinier van der Linden and Stefan van der Elst (Hubrecht Institute-KNAW, NL) for assistance
440 with FACS sorting experiments. We thank Klaas Mulder and Jan Gerlach for inspiring us to establish DSP
441 fixation for single cell RNA-sequencing, and for helpful practical suggestions. We thank Utrecht
442 Sequencing Facility for providing sequencing service and data. This work is financially supported by the
443 KWF Kankerbestrijding (Dutch Cancer Society, project grant 11941-2018-II) and ZonMW (grant
444 91116011). Further financial support was provided by research infrastructure grants from Utrecht Life
445 Sciences to the Single Cell Analysis Center and the Center for Cell Imaging. Utrecht Sequencing Facility is
446 subsidized by the University Medical Center Utrecht, Hubrecht Institute, Utrecht University and The
447 Netherlands X-omics Initiative (NWO project 184.034.019). We thank Alain de Bruin and the other
448 members of the Cancer Group for constructive feedback and suggestions.

449

450

451 **Author Contributions**

452 H.A.S. conceived and performed experiments, analyzed data, and wrote the manuscript. K.A.W.
453 conceived and performed experiments, analyzed data, and wrote the manuscript. E.A.v.L performed
454 experiments and analyzed data. F.M.R. analyzed single cell RNA-sequencing data. B.W. conceived and
455 oversaw the study and wrote the manuscript.

456

457 **Competing Interests**

458 The authors declare no competing interests.

459

460 **Data Availability**

461 All sequencing data is available at GEO under accession number GSE256134 for fresh and RAID-fixed cells
462 (Figure 2) and accession number GSE250285 for RAID-fixed cells sorted by γ H2AX level (Figure 3).

463

464 **Figure Legends**

465 **Figure 1: γ H2AX is a replication stress marker suitable for flow cytometry of DSP-fixed cells.**

466 **A** Schematic overview of the technique to combine immunostaining and single-cell RNA sequencing.
467 Cells are fixed with DSP, permeabilized and stained using fluorescent antibodies. Next, cells are sorted
468 based on fluorescent intensity. After de-crosslinking, cells are subjected to single-cell RNA sequencing.

469 **B** Flow cytometry data showing the intensity of potential RS markers in individual RPE-HRAS^{G12V} cells
470 treated for 24 hours with 10 nM CHK1i + 100nM gemcitabine or vehicle (Veh). Unstained control refers
471 to control cells not incubated or, when applicable, incubated with the secondary antibody only. Inset
472 zooms in on cells stained for γ H2AX after treatment with CHK1i + gemcitabine to indicate heterogeneity
473 in γ H2AX level.

474 **C** Representative example of γ H2AX immunostaining on RPE-HRAS^{G12V} cells treated for 24 hours with 10
475 nM CHK1i + 4 nM gemcitabine or vehicle (Veh).

476 **D** Immunoblot showing synergistic induction of RS by 10 nM CHK1i + 4 nM gemcitabine in RPE-HRAS^{G12V}
477 cells, as indicated by phospho CHK1 S345 and γ H2AX. The absence of phosphorylation of CHK1 on its
478 autophosphorylation site S296 indicates effective inhibition by CHK1i.

479

480 **Figure 2: High quality single-cell RNA sequencing data of fixed cells with known level of replication** 481 **stress.**

482 **A** Violin plot representing the average numbers of genes detected per cell in fresh and DSP fixed RPE-
483 HRAS^{G12V} cells.

484 **B** Scatter plot showing the average gene expression in DSP fixed and fresh cells. R value indicates
485 Pearson Correlation. The red line indicates $x=y$.

486 **C** Scatter plot showing the correlation between the gene detection rate and average gene expression in
487 fresh and DSP fixed cells. R value indicates Pearson Correlation coefficient between fresh and DSP fixed
488 cells.

489 **D** Scatter plot showing the correlation between the coefficient of variation and average gene expression
490 in fresh and DSP fixed cells. R value indicates Pearson Correlation coefficient between fresh and DSP
491 fixed cells.

492 **E** Dimensionality reduction using tSNE of DSP-fixed cells. Cells are color coded according to γ H2AX signal.

493 **F** Feature plot in which cells on tSNE plot in E are color-coded according to mAG-Geminin₁₋₁₁₀ signal.

494 **G** Feature plots in which cells on tSNE plot in E are color coded according to the expression of S-phase
495 (*CDC6* and *E2F1*) or G2-phase (*PLK1* and *CCNB1*) markers.

496

497 **Figure 3: Identification of putative genes that correlate with replication stress tolerance.**

498 **A** Flow cytometry data of RPE-HRAS^{G12V} and control cells treated for 16 hours with 10 nM CHK1i + 4 nM
499 gemcitabine or vehicle (Veh) . Sorting strategy is shown: first S-phase cells were selected based on DAPI
500 signal. For drug treated cells equal number of cells with no, low, medium or high levels of γ H2AX were
501 sorted. The percentages of cells in these different categories before sorting are indicated and show an
502 increase in the cell population with high level of RS after treatment with CHK1i + gemcitabine.

503 **B** Dimensionality reduction using tSNE of all cells (HRAS^{G12V} and control) before and after treatment with
504 10 nM CHK1i + 4 nM gemcitabine shows separate clusters of cells.

505 **C** Feature plot in which cells on tSNE plot in B are color coded based on the different conditions.

506 **D** Feature plot in which cells on tSNE plot in B are color coded according to γ H2AX signal.

507 **E** Heatmap of genes differentially expressed and downregulated in RPE HRAS^{G12V} γ H2AX^{low} versus
508 γ H2AX^{high} control RPE cells 16 hours after treatment with 10 nM CHK1i + 4 nM gemcitabine.

509 **F** Heatmap of genes differentially expressed and upregulated in γ H2AX^{low} versus γ H2AX^{high} RPE HRAS^{G12V}
510 cells 16 hours after treatment with 10 nM CHK1i + 4 nM gemcitabine.

511

512 **Figure 4: Partial knockdown of FOXM1 improves tolerance to replication stress without affecting cell**
513 **proliferation.**

514 **A** Schematic representation of the experimental design to identify and validate putative RS-tolerance
515 genes.

516 **B** Relative *FOXM1* expression of RPE-HRAS^{G12V} following transfection with four individual siRNAs
517 targeting *FOXM1* (1 nM each) as measured by qPCR. Gene expression was normalized to the average of
518 two housekeeping genes (*GAPDH*, *18S*). Error bars indicate mean +/- SEM. Significant differences
519 determined by one-way ANOVA with Geisser Greenhouse correction followed by Dunnett's multiple
520 comparison test. **p<0.01, N = 3. Representative of 3 individual experiments.

521 **C** Flow cytometry data of RPE-HRAS^{G12V} cells which were arrested in G1-phase after 24 hours treatment
522 with a CDK4/6i and individual siRNAs against *FOXM1*. Subsequently, cells were released in the absence or
523 presence of 10 nM CHK1i + 4 nM gemcitabine and harvested after 14 hours to enrich for S/G2-phase
524 cells. DAPI staining was used to determine cell cycle progression (top row) and γ H2AX staining was used
525 to determine the degree of replication stress (bottom row). Number in bottom right corner of bottom
526 row plots indicates the Geminin₁₋₁₁₀⁺ cells as percentage of the total cells. Number in the top right corner
527 of bottom row plots indicates γ H2AX⁺ cells as a percentage of Geminin₁₋₁₁₀⁺ cells. Representative of 2
528 individual experiments.

529 **D** Outgrown colonies of RPE-HRAS^{G12V} cells transfected for 24 hr with siRNAs against FOXM1 followed by
530 treatment for 48 hr with the 2 nM CHK1i and 4 nM gemcitabine. After removing drug-containing media,
531 colonies were allowed to grow for 5 days. Error bars indicate mean +/- SEM. Representative of 2
532 individual experiments.

533 **E** Quantification of colonies presented in panel B, presented as the IntensityPercent, which takes into
534 account both the area covered by the cell growth as well as the pixel intensity of the covered area. This
535 was quantified using the ImageJ ColonyArea plug-in. Error bars indicate mean +/- SEM. Significant
536 differences were determined by ordinary One-way ANOVA followed by Dunnett's multiple comparison
537 test. *p<0.05, **p<0.01, N=3.

- 538 Atashpaz, S., Samadi Shams, S., Gonzalez, J.M., Sebestyén, E., Arghavanifard, N., Gnocchi, A., Albers, E.,
539 Minardi, S., Faga, G., Soffientini, P., Allievi, E., Cancila, V., Bachi, A., Fernández-Capetillo, Ó, Tripodo,
540 C., Ferrari, F., López-Contreras, A.J. & Costanzo, V. 2020, "ATR expands embryonic stem cell fate
541 potential in response to replication stress", *eLife*, vol. 9.
- 542 Baillie, K.E. & Stirling, P.C. 2021, "Beyond Kinases: Targeting Replication Stress Proteins in Cancer
543 Therapy", *Trends in cancer*, vol. 7, no. 5, pp. 430-446.
- 544 Bajar, B.T., Lam, A.J., Badiiee, R.K., Oh, Y., Chu, J., Zhou, X.X., Kim, N., Kim, B.B., Chung, M., Yablonovitch,
545 A.L., Cruz, B.F., Kulalert, K., Tao, J.J., Meyer, T., Su, X. & Lin, M.Z. 2016, "Fluorescent indicators for
546 simultaneous reporting of all four cell cycle phases", *Nature Methods*, vol. 13, no. 12, pp. 993-996.
- 547 Barger, C.J., Branick, C., Chee, L. & Karpf, A.R. 2019, "Pan-Cancer Analyses Reveal Genomic Features of
548 FOXM1 Overexpression in Cancer", *Cancers*, vol. 11, no. 2, pp. 251. doi: 10.3390/cancers11020251.
- 549 Bartkova, J., Rezaei, N., Liontos, M., Karakaidos, P., Kletsas, D., Issaeva, N., Vassiliou, L.F., Kolettas, E.,
550 Niforou, K., Zoumpourlis, V.C., Takaoka, M., Nakagawa, H., Tort, F., Fugger, K., Johansson, F.,
551 Sehested, M., Andersen, C.L., Dyrskjot, L., Ørntoft, T., Lukas, J., Kittas, C., Helleday, T., Halazonetis,
552 T.D., Bartek, J. & Gorgoulis, V.G. 2006, "Oncogene-induced senescence is part of the tumorigenesis
553 barrier imposed by DNA damage checkpoints", *Nature*, vol. 444, no. 7119, pp. 633-637.
- 554 Bélanger, F., Fortier, E., Dubé, M., Lemay, J., Buisson, R., Masson, J., Elsherbiny, A., Costantino, S.,
555 Carmona, E., Mes-Masson, A., Wurtele, H. & Drobetsky, E. 2018, "Replication Protein A Availability
556 during DNA Replication Stress Is a Major Determinant of Cisplatin Resistance in Ovarian Cancer
557 Cells", *Cancer Research*, vol. 78, no. 19, pp. 5561-5573.
- 558 Bertoli, C., Herlihy, A.E., Pennycook, B.R., Kriston-Vizi, J. & de Bruin, R.A.M. 2016, "Sustained E2F-
559 Dependent Transcription Is a Key Mechanism to Prevent Replication-Stress-Induced DNA Damage",
560 *Cell Reports*, vol. 15, no. 7, pp. 1412-1422.
- 561 Bianco, J.N., Bergoglio, V., Lin, Y., Pillaire, M., Schmitz, A., Gilhodes, J., Lusque, A., Mazières, J., Lacroix-
562 Triki, M., Roumeliotis, T.I., Choudhary, J., Moreaux, J., Hoffmann, J., Tourrière, H. & Pasero, P. 2019,
563 "Overexpression of Claspin and Timeless protects cancer cells from replication stress in a
564 checkpoint-independent manner", *Nature Communications*, vol. 10, no. 1, pp. 910.
- 565 Blosser, W.D., Dempsey, J.A., McNulty, A.M., Rao, X., Ebert, P.J., Lowery, C.D., Iversen, P.W., Webster,
566 Y.W., Donoho, G.P., Gong, X., Merzoug, F.F., Buchanan, S., Boehnke, K., Yu, C., You, X.T., Beckmann,
567 R.P., Wu, W., McNeely, S.C., Lin, A.B. & Martinez, R. 2020, "A pan-cancer transcriptome analysis
568 identifies replication fork and innate immunity genes as modifiers of response to the CHK1 inhibitor
569 prexasertib", *Oncotarget*, vol. 11, no. 3, pp. 216-236.
- 570 Branigan, T.B., Kozono, D., Schade, A.E., Deraska, P., Rivas, H.G., Sambel, L., Reavis, H.D., Shapiro, G.I.,
571 D'Andrea, A.D. & DeCaprio, J.A. 2021, "MMB-FOXM1-driven premature mitosis is required for CHK1
572 inhibitor sensitivity", *Cell reports*, vol. 34, no. 9, pp. 108808.

- 573 Chung, S., Vail, P., Witkiewicz, A.K. & Knudsen, E.S. 2019, "Coordinately Targeting Cell-Cycle Checkpoint
574 Functions in Integrated Models of Pancreatic Cancer", *Clinical Cancer Research: An Official Journal*
575 *of the American Association for Cancer Research*, vol. 25, no. 7; 10., pp. 2290-2304.
- 576 Fischer, M. 2017, "Census and evaluation of p53 target genes", *Oncogene*, vol. 36, no. 28, pp. 3943-3956.
- 577 Fischer, M., Grossmann, P., Padi, M. & DeCaprio, J.A. 2016, "Integration of TP53, DREAM, MMB-FOXM1
578 and RB-E2F target gene analyses identifies cell cycle gene regulatory networks", *Nucleic acids*
579 *research*, vol. 44, no. 13, pp. 6070-6086.
- 580 Gallo, D., Young, J.T.F., Fourtounis, J., Martino, G., Alvarez-Quilon, A., Bernier, C., Duffy, N.M., Papp, R.,
581 Roulston, A., Stocco, R., Szychowski, J., Veloso, A., Alam, H., Baruah, P.S., Fortin, A.B., Bowlan, J.,
582 Chaudhary, N., Desjardins, J., Dietrich, E., Fournier, S., Fugere-Desjardins, C., Goulet de Rugy, T.,
583 Leclaire, M., Liu, B., Bhaskaran, V., Mamane, Y., Melo, H., Nicolas, O., Singhanian, A., Szilard, R.K.,
584 Tkac, J., Yin, S.Y., Morris, S.J., Zinda, M., Marshall, C.G. & Durocher, D. 2022, "CCNE1 amplification is
585 synthetic lethal with PKMYT1 kinase inhibition", *Nature*, vol. 604, no. 7907, pp. 749-756.
- 586 Gerlach, J.P., van Buggenum, J.A.G., Tanis, S.E.J., Hogeweg, M., Heuts, B.M.H., Muraro, M.J., Elze, L.,
587 Rivello, F., Rakszewska, A., van Oudenaarden, A., Huck, W.T.S., Stunnenberg, H.G. & Mulder, K.W.
588 2019, "Combined quantification of intracellular (phospho-)proteins and transcriptomics from fixed
589 single cells", *Scientific Reports*, vol. 9, no. 1, pp. 1-10.
- 590 Gilad, O., Nabet, B.Y., Ragland, R.L., Schoppy, D.W., Smith, K.D., Durham, A.C. & Brown, E.J. 2010,
591 "Combining ATR suppression with oncogenic Ras synergistically increases genomic instability,
592 causing synthetic lethality or tumorigenesis in a dosage-dependent manner", *Cancer Research*, vol.
593 70, no. 23, pp. 9693-9702.
- 594 Goldman, A., Majumder, B., Dhawan, A., Ravi, S., Goldman, D., Kohandel, M., Majumder, P.K. &
595 Sengupta, S. 2015, "Temporally sequenced anticancer drugs overcome adaptive resistance by
596 targeting a vulnerable chemotherapy-induced phenotypic transition", *Nature communications*, vol.
597 6, no. 1, pp. 6139.
- 598 Goodarzi, A.A., Jeggo, P.A. & Kurka, T. 2011, "KAP-1 phosphorylation regulates CHD3 nucleosome
599 remodeling during the DNA double-strand break response", *Nature structural & molecular biology*,
600 vol. 18, no. 7, pp. 831-839.
- 601 Gorgoulis, V.G., Vassiliou, L.F., Karakaidos, P., Zacharatos, P., Kotsinas, A., Liloglou, T., Venere, M.,
602 Ditullio, R.A., Kastriakis, N.G., Levy, B., Kletsas, D., Yoneta, A., Herlyn, M., Kittas, C. & Halazonetis,
603 T.D. 2005, "Activation of the DNA damage checkpoint and genomic instability in human
604 precancerous lesions", *Nature*, vol. 434, no. 7035, pp. 907-913.
- 605 Guzman, C., Bagga, M., Kaur, A., Westermarck, J. & Abankwa, D. 2014, "ColonyArea: an ImageJ plugin to
606 automatically quantify colony formation in clonogenic assays", *PloS one*, vol. 9, no. 3, pp. e92444.
- 607 Hafemeister, C. & Satija, R. 2019, "Normalization and variance stabilization of single-cell RNA-seq data
608 using regularized negative binomial regression", *Genome Biology*, vol. 20, no. 1, pp. 296.

- 609 Hong, D.S., Moore, K., Patel, M., Grant, S.C., Burris, H.A., William, W.N., Jones, S., Meric-Bernstam, F.,
610 Infante, J., Golden, L., Zhang, W., Martinez, R., Wijayawardana, S., Beckmann, R., Lin, A.B., Eng, C. &
611 Bendell, J. 2018, "Evaluation of Prexasertib, a Checkpoint Kinase 1 Inhibitor, in a Phase Ib Study of
612 Patients with Squamous Cell Carcinoma", *Clinical Cancer Research: An Official Journal of the*
613 *American Association for Cancer Research*, vol. 24, no. 14, pp. 3263-3272.
- 614 Jo, U., Murai, Y., Chakka, S., Chen, L., Cheng, K., Murai, J., Saha, L.K., Miller Jenkins, L.M. & Pommier, Y.
615 2021, "SLFN11 promotes CDT1 degradation by CUL4 in response to replicative DNA damage, while
616 its absence leads to synthetic lethality with ATR/CHK1 inhibitors", *Proceedings of the National*
617 *Academy of Sciences of the United States of America*, vol. 118, no. 6, pp. e2015654118. doi:
618 10.1073/pnas.2015654118.
- 619 Katsuno, Y., Suzuki, A., Sugimura, K., Okumura, K., Zineldeen, D.H., Shimada, M., Niida, H., Mizuno, T.,
620 Hanaoka, F. & Nakanishi, M. 2009, "Cyclin A-Cdk1 regulates the origin firing program in mammalian
621 cells", *Proceedings of the National Academy of Sciences of the United States of America*, vol. 106,
622 no. 9, pp. 3184-3189.
- 623 Koh, S., Wallez, Y., Dunlop, C.R., Bernaldo de Quiros Fernandez, S., Bapiro, T.E., Richards, F.M. & Jodrell,
624 D.I. 2018, "Mechanistic Distinctions between CHK1 and WEE1 Inhibition Guide the Scheduling of
625 Triple Therapy with Gemcitabine", *Cancer research*, vol. 78, no. 11, pp. 3054-3066.
- 626 Lecona, E. & Fernandez-Capetillo, O. 2018, "Targeting ATR in cancer", *Nature reviews. Cancer*, vol. 18, no.
627 9, pp. 586-595.
- 628 Liu, Y., Li, Y., Wang, X., Liu, F., Gao, P., Quinn, M.M., Li, F., Merlino, A.A., Benes, C., Liu, Q., Gray, N.S. &
629 Wong, K. 2017, "Gemcitabine and Chk1 Inhibitor AZD7762 Synergistically Suppress the Growth of
630 Lkb1-Deficient Lung Adenocarcinoma", *Cancer Research*, vol. 77, no. 18, pp. 5068-5076.
- 631 Macheret, M. & Halazonetis, T.D. 2015a, "DNA replication stress as a hallmark of cancer", *Annual review*
632 *of pathology*, vol. 10, pp. 425-448.
- 633 Macheret, M. & Halazonetis, T.D. 2015b, "DNA replication stress as a hallmark of cancer", *Annual Review*
634 *of Pathology*, vol. 10, pp. 425-448.
- 635 Menolfi, D., Lee, B.J., Zhang, H., Jiang, W., Bowen, N.E., Wang, Y., Zhao, J., Holmes, A., Gershik, S.,
636 Rabadan, R., Kim, B. & Zha, S. 2023, "ATR kinase supports normal proliferation in the early S phase
637 by preventing replication resource exhaustion", *Nature communications*, vol. 14, no. 1, pp. 3618-5.
- 638 Mukhopadhyay, S., Goswami, D., Adisheshaiah, P.P., Burgan, W., Yi, M., Guerin, T.M., Kozlov, S.V., Nissley,
639 D.V. & McCormick, F. 2020, "Undermining Glutaminolysis Bolsters Chemotherapy While NRF2
640 Promotes Chemoresistance in KRAS-Driven Pancreatic Cancers", *Cancer Research*, vol. 80, no. 8, pp.
641 1630-1643.
- 642 Murga, M., Campaner, S., Lopez-Contreras, A.J., Toledo, L.I., Soria, R., Montaña, M.F., Artista, L.D.,
643 Schleker, T., Guerra, C., Garcia, E., Barbacid, M., Hidalgo, M., Amati, B. & Fernandez-Capetillo, O.
644 2011, "Exploiting oncogene-induced replicative stress for the selective killing of Myc-driven
645 tumors", *Nature Structural & Molecular Biology*, vol. 18, no. 12, pp. 1331-1335.

- 646 O'Brien, S., Ubhi, T., Wolf, L., Gandhi, K., Lin, S., Chaudary, N., Dhani, N.C., Milosevic, M., Brown, G.W. &
647 Angers, S. 2023, "FBXW7-loss Sensitizes Cells to ATR Inhibition Through Induced Mitotic
648 Catastrophe", *Cancer research communications*, vol. 3, no. 12, pp. 2596-2607.
- 649 Oo, Z.Y., Stevenson, A.J., Proctor, M., Daignault, S.M., Walpole, S., Lanagan, C., Chen, J., Škalamera, D.,
650 Spoerri, L., Ainger, S.A., Sturm, R.A., Haass, N.K. & Gabrielli, B. 2018, "Endogenous Replication Stress
651 Marks Melanomas Sensitive to CHEK1 Inhibitors In Vivo", *Clinical Cancer Research: An Official
652 Journal of the American Association for Cancer Research*, vol. 24, no. 12, pp. 2901-2912.
- 653 Parekh, S., Ziegenhain, C., Vieth, B., Enard, W. & Hellmann, I. 2018, "zUMIs - A fast and flexible pipeline
654 to process RNA sequencing data with UMIs", *GigaScience*, vol. 7, no. 6.
- 655 Rehman, S.K., Haynes, J., Collignon, E., Brown, K.R., Wang, Y., Nixon, A.M.L., Bruce, J.P., Wintersinger,
656 J.A., Singh Mer, A., Lo, E.B.L., Leung, C., Lima-Fernandes, E., Pedley, N.M., Soares, F., McGibbon, S.,
657 He, H.H., Pollet, A., Pugh, T.J., Haibe-Kains, B., Morris, Q., Ramalho-Santos, M., Goyal, S., Moffat, J.
658 & O'Brien, C.A. 2021, "Colorectal Cancer Cells Enter a Diapause-like DTP State to Survive
659 Chemotherapy", *Cell*, vol. 184, no. 1, pp. 226-242.e21.
- 660 Ruiz, S., Mayor-Ruiz, C., Lafarga, V., Murga, M., Vega-Sendino, M., Ortega, S. & Fernandez-Capetillo, O.
661 2016, "A Genome-wide CRISPR Screen Identifies CDC25A as a Determinant of Sensitivity to ATR
662 Inhibitors", *Molecular cell*, vol. 62, no. 2, pp. 307-313.
- 663 Sadasivam, S., Duan, S. & DeCaprio, J.A. 2012, "The MuvB complex sequentially recruits B-Myb and
664 FoxM1 to promote mitotic gene expression", *Genes & development*, vol. 26, no. 5, pp. 474-489.
- 665 Sanders, D.A., Gormally, M.V., Marsico, G., Beraldi, D., Tannahill, D. & Balasubramanian, S. 2015,
666 "FOXM1 binds directly to non-consensus sequences in the human genome", *Genome biology*, vol.
667 16, no. 1, pp. 130-z.
- 668 Schleicher, E.M., Dhoonmoon, A., Jackson, L.M., Clements, K.E., Stump, C.L., Nicolae, C.M. & Moldovan,
669 G. 2020, "Dual genome-wide CRISPR knockout and CRISPR activation screens identify mechanisms
670 that regulate the resistance to multiple ATR inhibitors", *PLOS Genetics*, vol. 16, no. 11, pp.
671 e1009176.
- 672 Schoppy, D.W., Ragland, R.L., Gilad, O., Shastri, N., Peters, A.A., Murga, M., Fernandez-Capetillo, O.,
673 Diehl, J.A. & Brown, E.J. 2012, "Oncogenic stress sensitizes murine cancers to hypomorphic
674 suppression of ATR", *The Journal of Clinical Investigation*, vol. 122, no. 1, pp. 241-252.
- 675 Segeren, H.A., van Liere, E.A., Riemers, F.M., de Bruin, A. & Westendorp, B. 2022, "Oncogenic RAS
676 sensitizes cells to drug-induced replication stress via transcriptional silencing of P53", *Oncogene*,
677 vol. 41, no. 19, pp. 2719-2733.
- 678 Seth, S., Li, C., Ho, I.-., Corti, D., Loponte, S., Sapio, L., Del Poggetto, E., Yen, E., Robinson, F.S., Peoples,
679 M., Karpinets, T., Deem, A.K., Kumar, T., Song, X., Jiang, S., Kang, Y., Fleming, J., Kim, M., Zhang, J.,
680 Maitra, A., Heffernan, T.P., Giuliani, V., Genovese, G., Futreal, A., Draetta, G.F., Carugo, A. & Viale, A.
681 2019, "Pre-existing Functional Heterogeneity of Tumorigenic Compartment as the Origin of
682 Chemoresistance in Pancreatic Tumors", *Cell Reports*, vol. 26, no. 6, pp. 1518-1532.e9.

- 683 Shaffer, S.M., Dunagin, M.C., Torborg, S.R., Torre, E.A., Emert, B., Krepler, C., Beqiri, M., Sproesser, K.,
684 Brafford, P.A., Xiao, M., Eggan, E., Anastopoulos, I.N., Vargas-Garcia, C.A., Singh, A., Nathanson, K.L.,
685 Herlyn, M. & Raj, A. 2017, "Rare cell variability and drug-induced reprogramming as a mode of
686 cancer drug resistance", *Nature (London)*, vol. 546, no. 7658, pp. 431-435.
- 687 Stuart, T., Butler, A., Hoffman, P., Hafemeister, C., Papalexi, E., Mauck, W.M., Hao, Y., Stoeckius, M.,
688 Smibert, P. & Satija, R. 2019, "Comprehensive Integration of Single-Cell Data", *Cell*, vol. 177, no. 7,
689 pp. 1888-1902.e21.
- 690 Toledo, L., Altmeyer, M., Rask, M., Lukas, C., Larsen, D., Povlsen, L., Bekker-Jensen, S., Mailand, N.,
691 Bartek, J. & Lukas, J. 2013, "ATR Prohibits Replication Catastrophe by Preventing Global Exhaustion
692 of RPA", *Cell (Cambridge)*, vol. 155, no. 5, pp. 1088-1103.
- 693 Wallez, Y., Dunlop, C.R., Johnson, T.I., Koh, S., Fornari, C., Yates, J.W.T., Bernaldo de Quirós Fernández, S.,
694 Lau, A., Richards, F.M. & Jodrell, D.I. 2018, "The ATR Inhibitor AZD6738 Synergizes with Gemcitabine
695 In Vitro and In Vivo to Induce Pancreatic Ductal Adenocarcinoma Regression", *Molecular Cancer
696 Therapeutics*, vol. 17, no. 8, pp. 1670-1682.
- 697

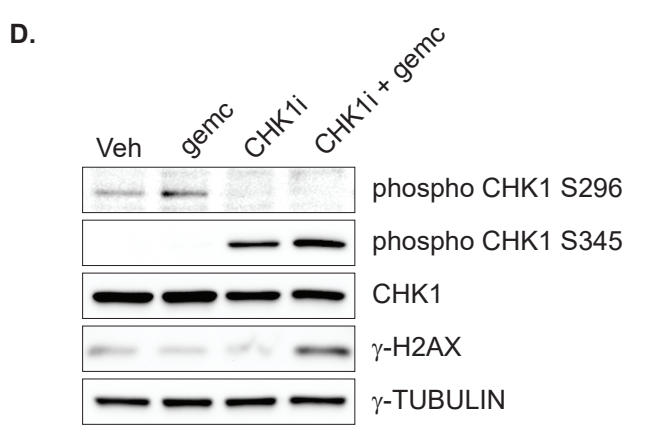
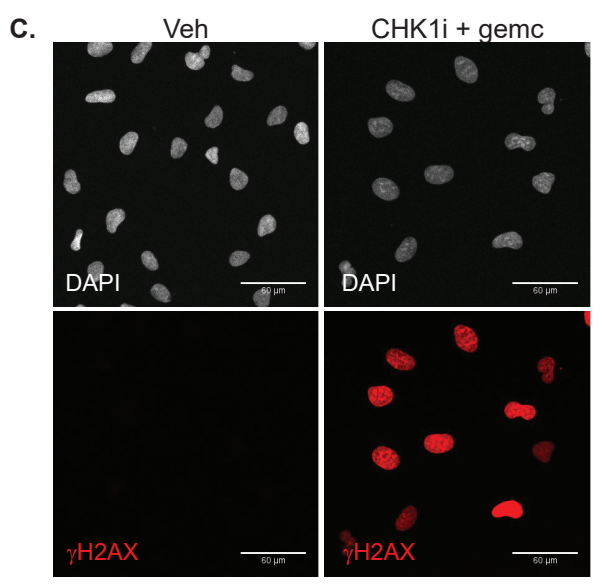
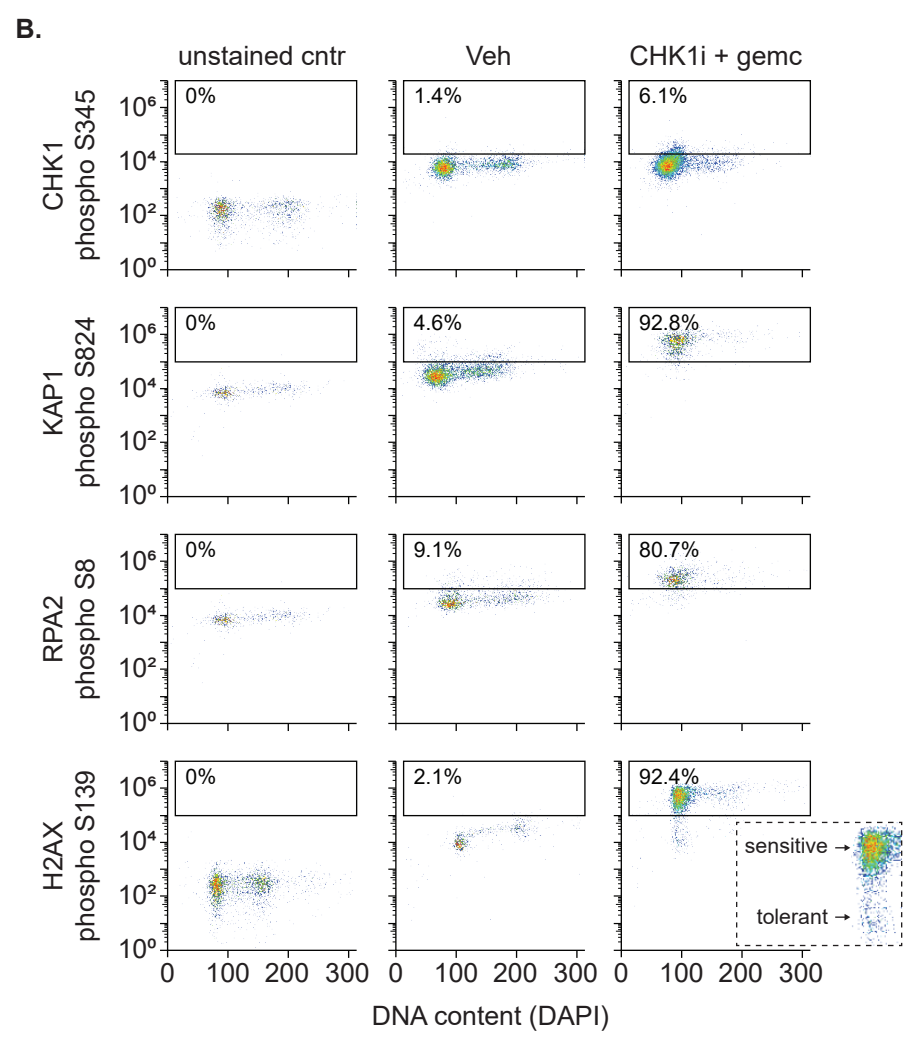
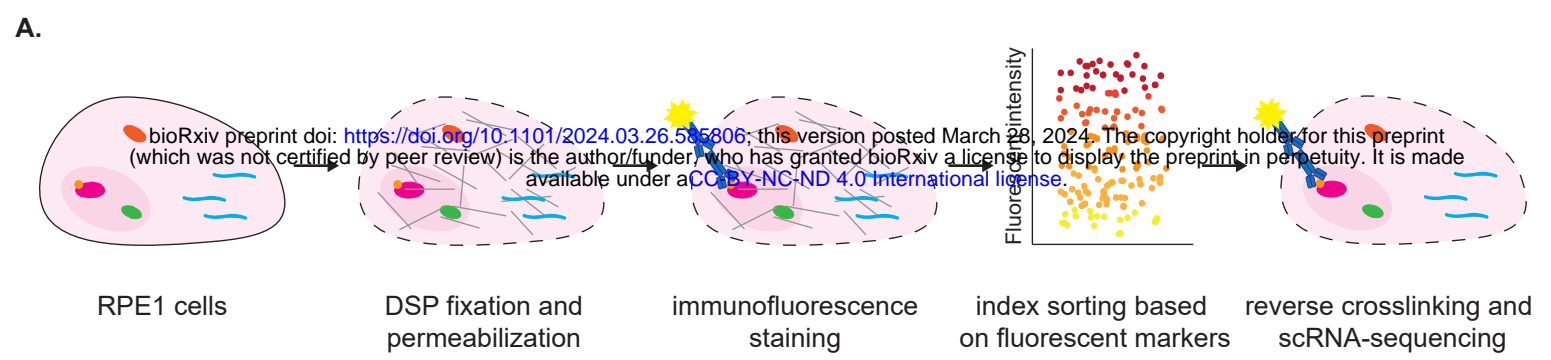


Figure 1: γ H2AX is a replication stress marker suitable for flowcytometry of DSP-fixed cells

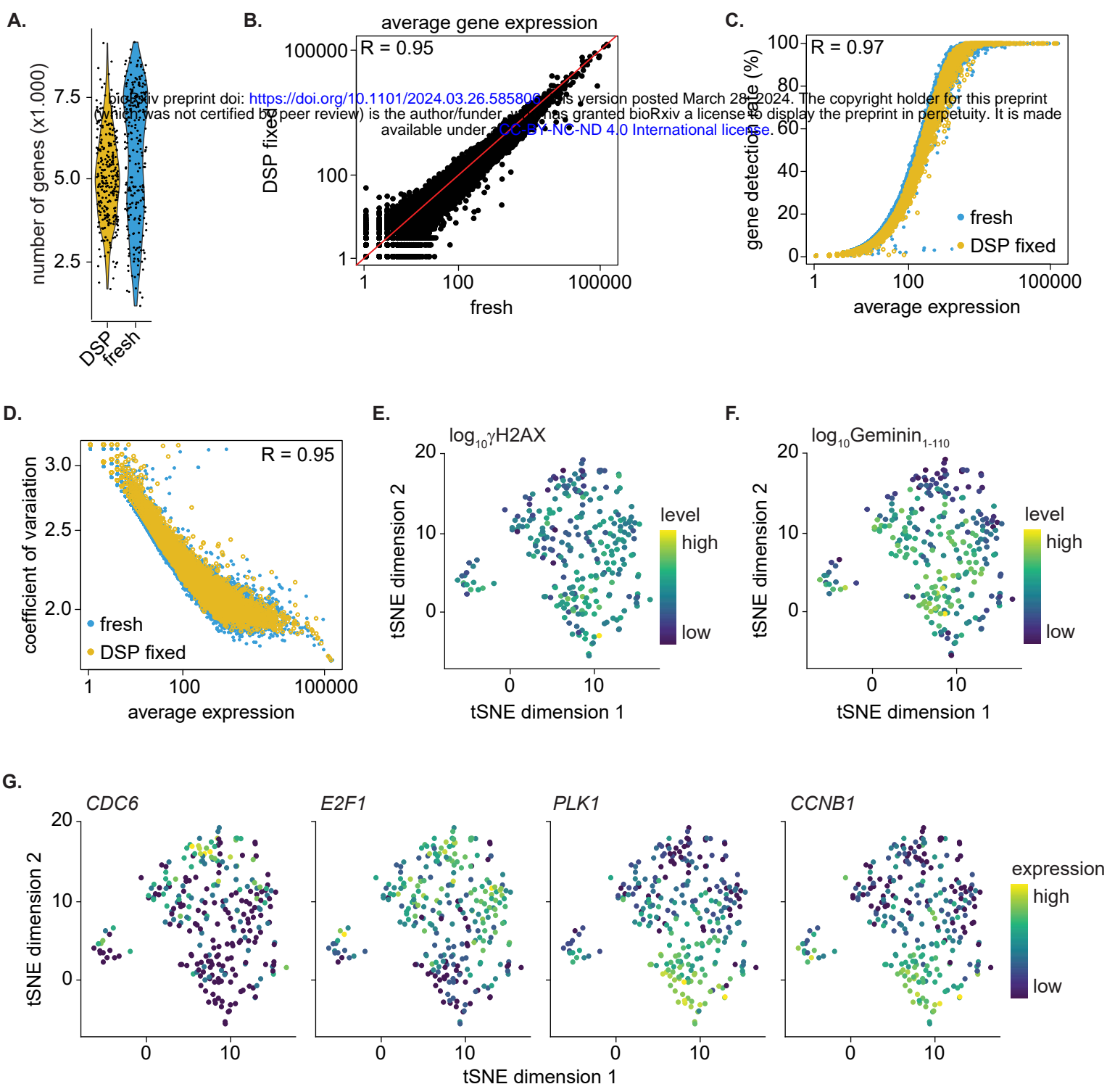


Figure 2: High-quality single-cell RNA sequencing data of fixed cells with known level of replication stress.

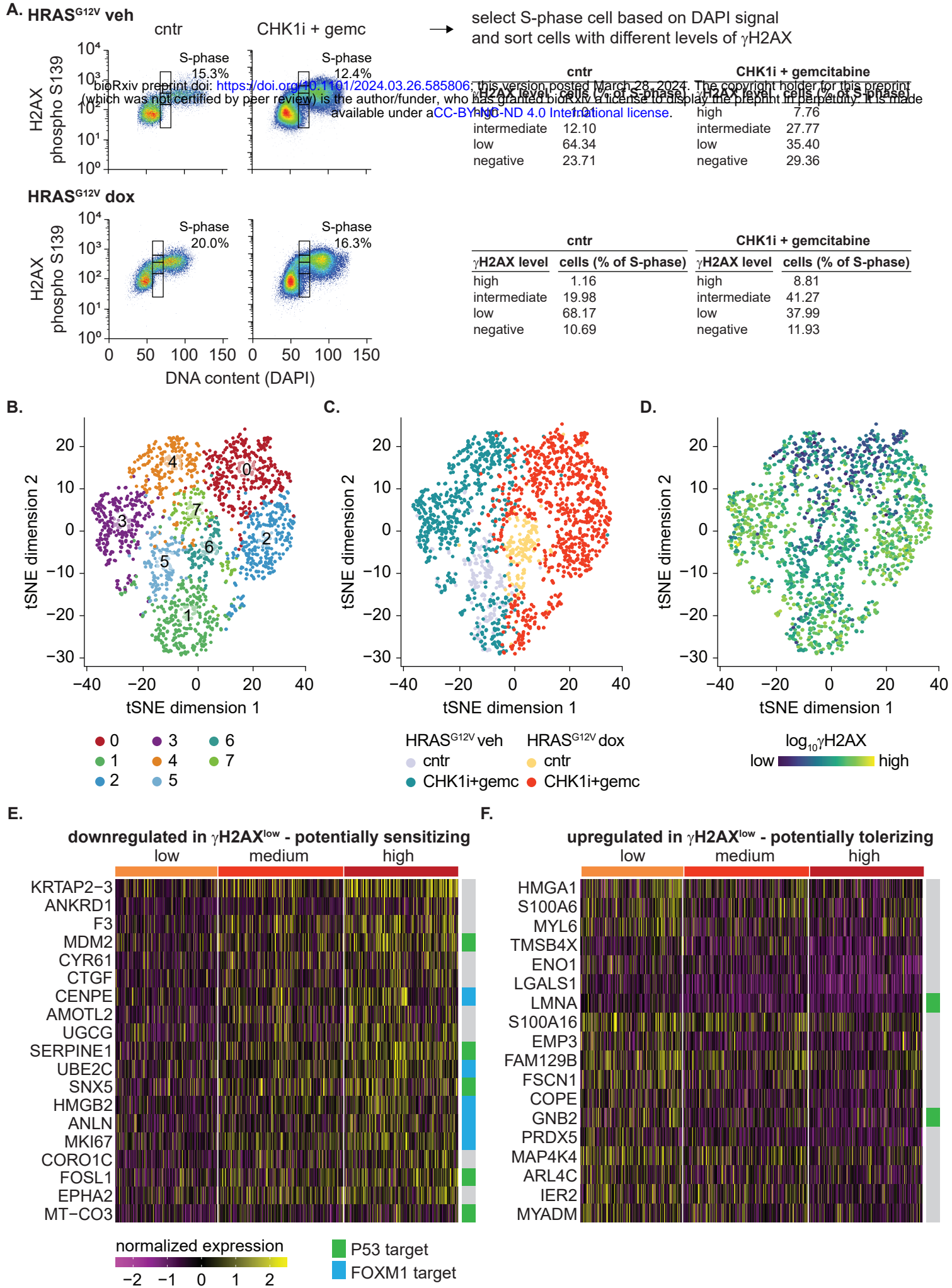


Figure 3: Identification of putative genes that confer replication stress tolerance.

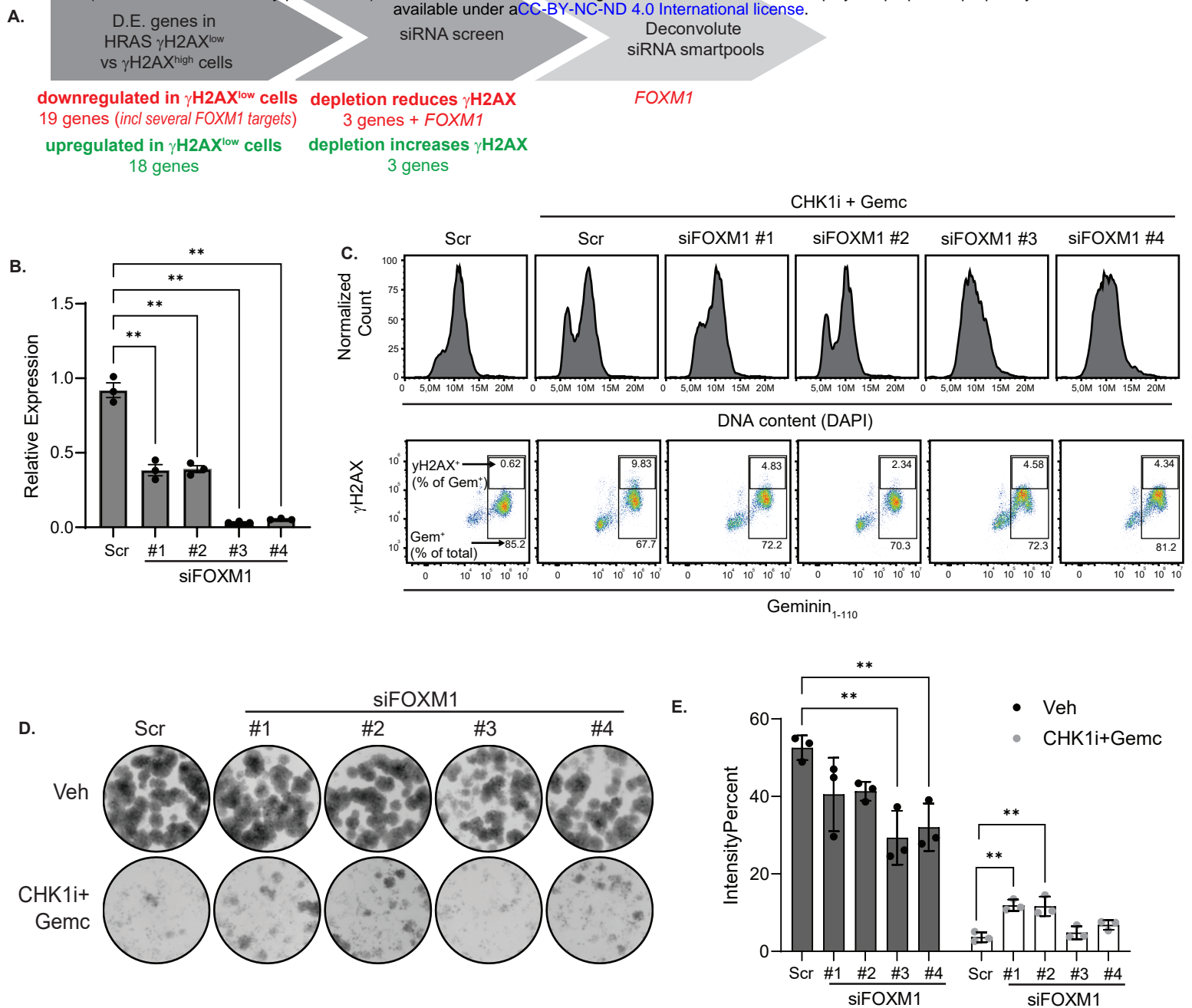


Figure 4: Partial knockdown of *FOXM1* improves tolerance to replication stress without affecting cell proliferation.